Description of complex time series by multipoles

M. Lewkowicz[a,*], J. Levitan[a,b], N. Puzanov[c],
N. Shnerb[a], K. Saermark[b]

[a]*Department of Physics, College of Judea and Samaria, Ariel 44837, Israel*
[b]*Department of Physics, The Technical University of Denmark, DK 2800 Lyngby, Denmark*
[c]*The Technological Incubator, Ariel 44837, Israel*

Abstract

We present a new method to describe time series with a highly complex time evolution. The time series is projected onto a two-dimensional phase–space plot which is quantified in terms of a multipole expansion where every data point is assigned a unit mass. The multipoles provide an efficient characterization of the original time series. © 2002 Elsevier Science B.V. All rights reserved.

1. Introduction

Up to now, two different measures of HRV analysis have been applied in the medical research: (a) Scale-dependent measures as SDNN (the standard deviation of the beat-to-beat interval time series); the standard deviation of the multiresolution wavelet transform as used by Turner et al. [1]; the standard deviation of the detrended time series as defined by Ashkenazy et al. [2], and (b) scale-independent measures (as the scaling exponent of the detrended fluctuations (DFA) as introduced by Peng et al. [3]).

Both methods have shown limited applicability individually [4–6], but rather a combination of both is necessary [7].

In clinical medicine, the dynamics of the beat-to-beat (RR) time series is commonly represented by a phase–space (or recurrence) plot, where each R–R interval is plotted against the previous one. The classification of the phase–space plots is traditionally

---

* Corresponding author. Fax: +972-3-9066161.
  E-mail address: lewkow@ycariel.yosh.ac.il (M. Lewkowicz).

performed by visual inspection and semi-quantitative analysis of the various measures describing the features of the plot, as the length or width [8–10]. But, as pointed out by Malik [11], this approach ignores the varying density of points leading to similar plots due to hearts with very different dynamics.

In this article, we present a new way to investigate phase–space plots from complex time series. In our analysis we calculate measures and parameters, which describe the features of the plot. The advantages of the method will become evident when applying it to well-known dynamical systems. By applying the method to the DIAMOND study [12] we shall demonstrate that these measures and parameters have more prognostic power than previous suggested risk markers.

2. The multipoles

We interpret the two-dimensional phase–space plot as a two-dimensional body where each data point is assigned a unit mass. The distribution of points will be expressed by the various moments known from (gravitational) potential theory.

The monopole M represents the total mass, i.e., the number of data points. The gravitational dipole moment vanishes by choosing the origin of the coordinate system in the centre of mass. As the quadrupole tensor is traceless, we may restrict ourselves to the following form:

$$Q_{ij} = \begin{pmatrix} Q_{xx} & 0 \\ 0 & Q_{yy} \end{pmatrix} \tag{1}$$

and $Q_{zz} = -(Q_{xx} + Q_{yy})$, where $Q_{xx} = \sum_\alpha (2x_\alpha^2 - y_\alpha^2)$ and $Q_{yy} = \sum_\alpha (2y_\alpha^2 - x_\alpha^2)$; the sums are over all the data points.

Here, the x and y coordinates of the data points are measured in the principal coordinate system, where the off-diagonal terms of the Q_{ij} tensor vanish. These axis are positioned in praxis for beat-to-beat time series along and vertical to the diagonal of the original phase–space plot.

Similarly, the octupole moments (with $z = 0$) in the principal axis coordinate are given by

$$T_{xxx} = \sum_\alpha (6x_\alpha^3 - 9x_\alpha y_\alpha^2),$$

$$T_{yyy} = \sum_\alpha (6y_\alpha^3 - 9x_\alpha^2 y_\alpha),$$

$$T_{xxy} = \sum_\alpha (36x_\alpha^2 y_\alpha - 9y_\alpha^3),$$

$$T_{xyy} = \sum_\alpha (36x_\alpha^2 y_\alpha - 9y_\alpha^3),$$

$$T_{xzz} = \sum_\alpha (-9x_\alpha y_\alpha^2 - 9x_\alpha^3),$$

$$T_{yzz} = \sum_{\alpha}(-9x_\alpha^2 y_\alpha - 9y_\alpha^3)\,. \tag{2}$$

Since $T_{yzz} + T_{xxy} = -3T_{yyy}$ and $T_{xyy} + T_{xzz} = -3T_{xxx}$, there are only four independent octupole measures.

Finally, the hexadecapole moments (with $z = 0$) in the principal axis coordinate system are

$$H_{xxxx} = \sum_{\alpha}(24x_\alpha^4 - 72x_\alpha^2 y_\alpha^2 + 9y_\alpha^4)\,,$$

$$H_{xxxy} = \sum_{\alpha}(240x_\alpha^3 y_\alpha - 180x_\alpha y_\alpha^3)\,,$$

$$H_{xxyy} = \sum_{\alpha}(-72x_\alpha^4 + 486x_\alpha^2 y_\alpha^2 - 72y_\alpha^4)\,,$$

$$H_{xyyy} = \sum_{\alpha}(-180x_\alpha^3 y_\alpha + 240x_\alpha y_\alpha^3)\,,$$

$$H_{yyyy} = \sum_{\alpha}(9x_\alpha^4 - 72x_\alpha^2 y_\alpha^2 + 24y_\alpha^4)\,,$$

$$H_{xxzz} = \sum_{\alpha}(-72x_\alpha^4 - 72x_\alpha^2 y_\alpha^2 + 9y_\alpha^4)\,,$$

$$H_{yyzz} = \sum_{\alpha}(18x_\alpha^4 - 54x_\alpha^2 y_\alpha^2 - 72y_\alpha^4)\,,$$

$$H_{xyzz} = \sum_{\alpha}(-180x_\alpha^3 y_\alpha - 180x_\alpha y_\alpha^3) \tag{3}$$

and since $H_{xxxy} + H_{xyyy} = -1/3\ H_{xyzz}$ and $H_{xxzz} + H_{yyzz} = -6H_{zzzz}$, there are only six independent hexadecapole measures.

For the purpose of elucidating these multipoles, we demonstrate their characteristics on distributions $D(x, y)$ that are reminiscent of actual density distributions from ECG recordings.

In Fig. 1, we show the distributions along the x and y axis, respectively, for a typical phase–space plot of a 24-h Holter recording, where all the points were projected along the x- or y-axis, respectively. To a first approximation they can be described by Gaussian distributions, with σ_x and σ_y as standard deviations along the x- and y-axis, respectively. Therefore, we consider as a first example the density distribution as a product of two Gaussians.

The quadrupole measures are then given by

$$Q_{xx} = \int\int(2x^2 - y^2)D(x, y)\,dx\,dy = 2\sigma_x^2 - \sigma_y^2\,,$$

$$Q_{yy} = \int\int(2y^2 - x^2)D(x, y)\,dx\,dy = 2\sigma_y^2 - \sigma_x^2\,. \tag{4}$$

Whereas in three dimensions a homogenous sphere has only zero quadrupole moments, its projection on the plane has a Gaussian mass distribution along the radial direction.
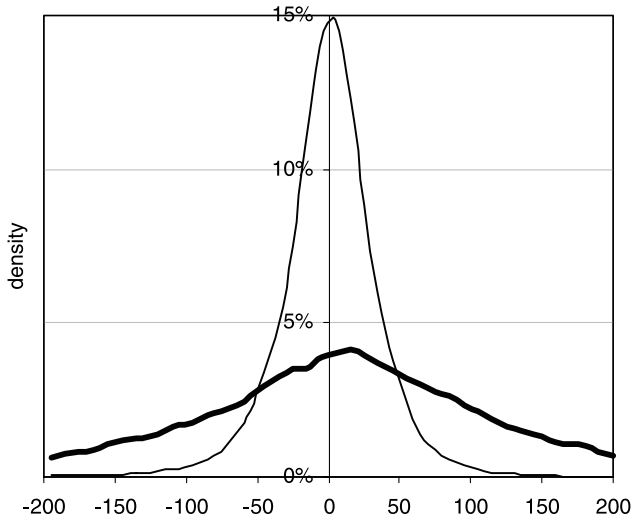
Fig. 1. The projected distributions along the x (lower curve) and y-axis (upper curve), respectively, for a typical phase–space plot of a 24-h Holter recording from a healthy individual.

If the projection is on the x–y plane one has a phase–space plot with a circular shape where the density of points decreases with increasing distance from the origin with $\sigma_x = \sigma_y$. In this case both principal quadrupole moments are positive.

A vanishing quadrupole moment, for example Q_{yy}, is obtained for $\sigma_x = \sqrt{2}\sigma_y$, which defines a reference ellipse in two dimensions; here $Q_{xx} = 3\sigma_y^2$. Varying the σ_x/σ_y ratio, one obtains more or less elongated ellipses along the x-axis or y-axis, depending on $\sigma_x/\sigma_y\sqrt{2}$.

For a symmetrical distribution as the Gaussian distribution the octupole moments vanish. We choose as a model distribution along the x-axis the normalized double exponential distributions

$$E(x) = \frac{\exp\{-\lambda_x x - e^{-x}\}}{\Gamma(\lambda_x)} \tag{5a}$$

and

$$\exists(x) = \frac{\exp\{\lambda_x x - e^{x}\}}{\Gamma(\lambda_x)} \,, \tag{5b}$$

where the parameter λ_x can obtain positive values and $\Gamma(\lambda_x)$ is the Gamma function.

Similar distribution can be defined along the y-axis. A few curves with various λ's are shown in Fig. 2. These distributions are non-symmetric; the degree of the deviation from symmetry is defined by the skewness γ, which is defined for any distribution $\phi(x)$ by

$$\gamma = \frac{\int_{-\infty}^{\infty} \bar{x}^3 \phi(x)\,\mathrm{d}x}{\sigma_x^3} \,, \tag{6}$$
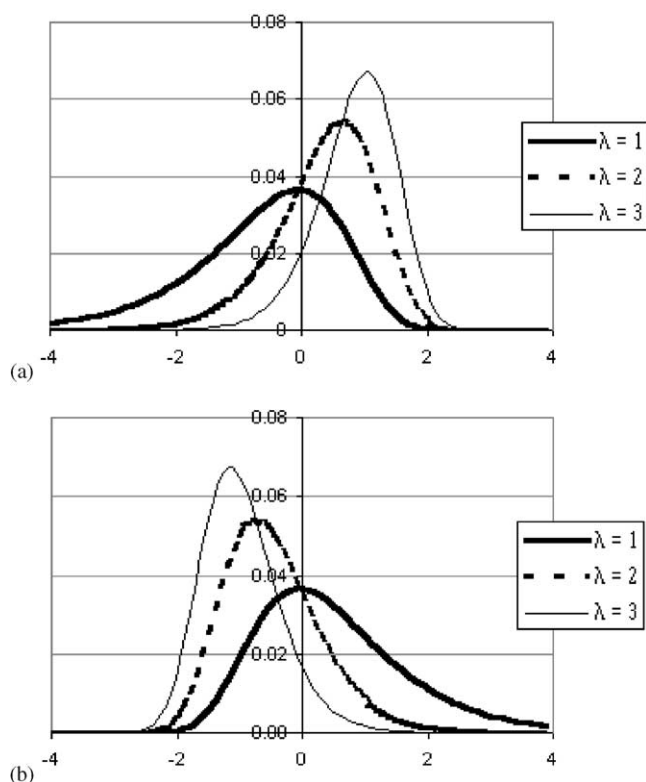
Fig. 2. The double exponential distributions: (a) $E(x)$, (b) $\exists(x)$ for $\lambda = 1, 2, 3$.

with σ_x being the standard deviation of the distribution. For $E(x)$ the skewness is positive, while for $\exists(x)$ it is negative.

The quadrupole moments with these distributions are still as in Eqs. (4), where the variance is now a function of λ:

$$\sigma^2 = \Psi^{(1)}(\lambda) \,. \tag{7}$$

$\Psi^{(1)}(\lambda)$ is the Trigamma function; in general, the Polygamma functions are defined as

$$\Psi^{(n)}(\lambda) = \frac{\mathrm{d}^{n+1}}{\mathrm{d}\lambda^{n+1}} \ln \Gamma(\lambda) \,. \tag{8}$$

The octupole moments are given by

$$
\begin{aligned}
T_{xxx} &= \mp 6 \Psi^{(2)}(\lambda_x) \,, \\
T_{yyy} &= \mp 6 \Psi^{(2)}\left(\lambda_y\right) \,, \\
T_{xyy} &= \pm 9 \Psi^{(2)}\left(\lambda_x\right) \,, \\
T_{xxy} &= \pm 9 \Psi^{(2)}\left(\lambda_y\right) \,.
\end{aligned}
\tag{9}
$$

The upper sign applies for $E(x)$ and the lower for $\exists(x)$.

These moments can be also expressed in terms of the skewness:

$$T_{xxx} = 6\gamma_x\sigma_x^3,$$
$$T_{yyy} = 6\gamma_y\sigma_y^3,$$
$$T_{xyy} = -9\gamma_x\sigma_x^3,$$
$$T_{xxy} = -9\gamma_y\sigma_y^3. \tag{10}$$

The hexadecapole moments are rather cumbersome to interpret, hence we choose to employ the kurtosis [13], which is related to the hexadecapole moments:

$$\kappa_x = \frac{\int_{-\infty}^{\infty} \bar{x}^4 \phi(x)\,\mathrm{d}x}{\sigma_x^4} - 3. \tag{11}$$

The kurtosis is negative for a flat topped distribution, vanishes for a Gaussian distribution and is positive for a sharp peaked distribution. For both double exponential distributions it is given by

$$\kappa = \frac{\Psi^{(3)}(\lambda)}{[\Psi^{(1)}(\lambda)]^2}. \tag{12}$$

3. Application to a non-linear system

We shall in the following consider a simple non-linear system for ordinary differential equations with time varying attractor dimension. Such a system was treated by Saermark et al. [14].

The model is defined by the equations

$$\frac{\mathrm{d}x}{\mathrm{d}t} = \alpha(-y-z) + \beta\sigma(y-y_0-x+x_0),$$

$$\frac{\mathrm{d}y}{\mathrm{d}t} = \alpha(x+ay) + \beta((x_0-x)(z-z_0) + r(x-x_0) + y_0 - y),$$

$$\frac{\mathrm{d}z}{\mathrm{d}t} = \alpha(b+z(x-c)) + \beta((x-x_0)(y-y_0) - B(z-z_0)). \tag{13}$$

The system reduces to the well-known Rössler system for $\alpha = 1$ and $\beta = 0$ and to the Lorenz system for $\alpha = 0$ and $\beta = 1$. In Ref. [14] we confined the examination of this system to the unit circle $\alpha^2 + \beta^2 = 1$ and investigated more closely the time evolution for the system when α is fixed, $\alpha = 0.037005$. The parameters for system (13) employed in Ref. [14] are given in Table 1.

In Fig. 3 (taken from Ref. [14]), we display the trajectory for three different intervals.

For the first 60 000 data points the trajectory is a limit cycle. A time local dimension was calculated for this segment and was found to be 1.35.

The next 255 400 data points exhibit a typical Lorenz-like behaviour, which however is limited in time and followed by an approach to a fixed point (the last 85 000 data points). While the Lorenz-like segment may be characterized by a dimension of 1.78, the last segment can obviously not be ascribed any dimension.

Table 1
The parameters for system (13)

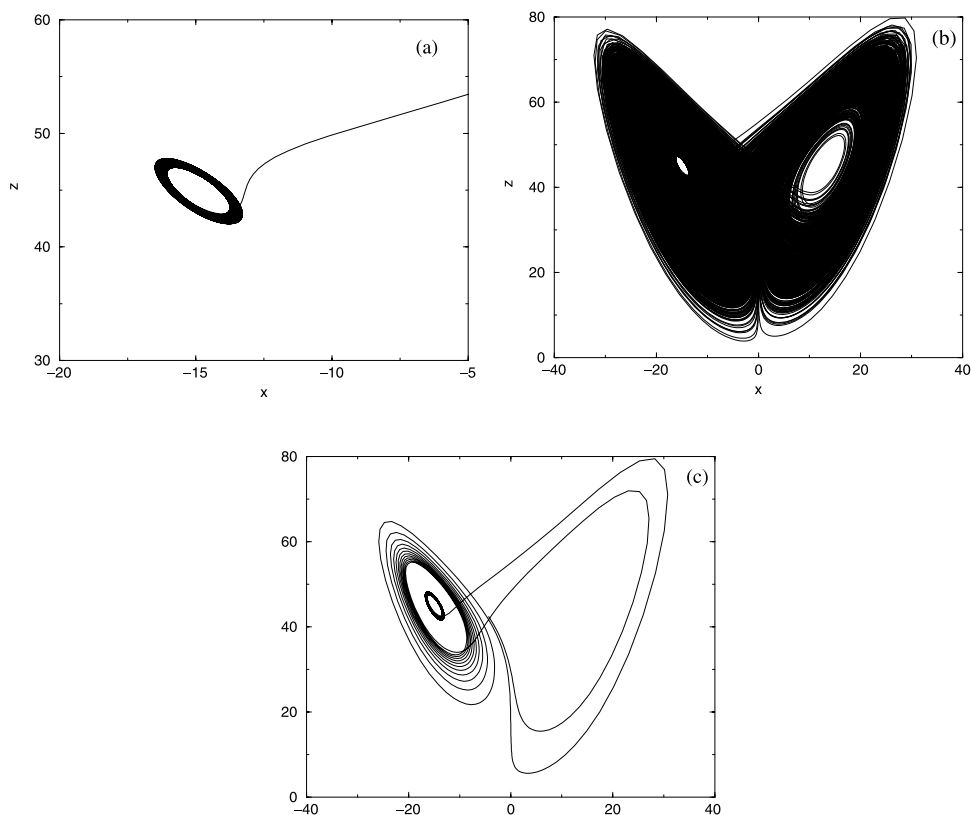|	
a	0.15
b	0.20
c	10.00
r	45.92
B	4.00
σ	16.00
x_0	-0.003001
y_0	0.02001
z_0	-0.02001

Fig. 3. The trajectory for the system (12) for the three different intervals: (a) 1–60000 data points, (b) 60001–315000, (c) 315001–400000.

In Ref. [14], Fig. 4a, outbursts of strong and intermittent oscillations of the *x*-component are apparent. They coincide precisely with the transitions from more stable to more complex types of trajectories and are repeated during the transition from the Lorenz-like attractor to the approach to a fixed point. This varying behaviour underlines the need for a more time-sensitive mode of description of such systems.
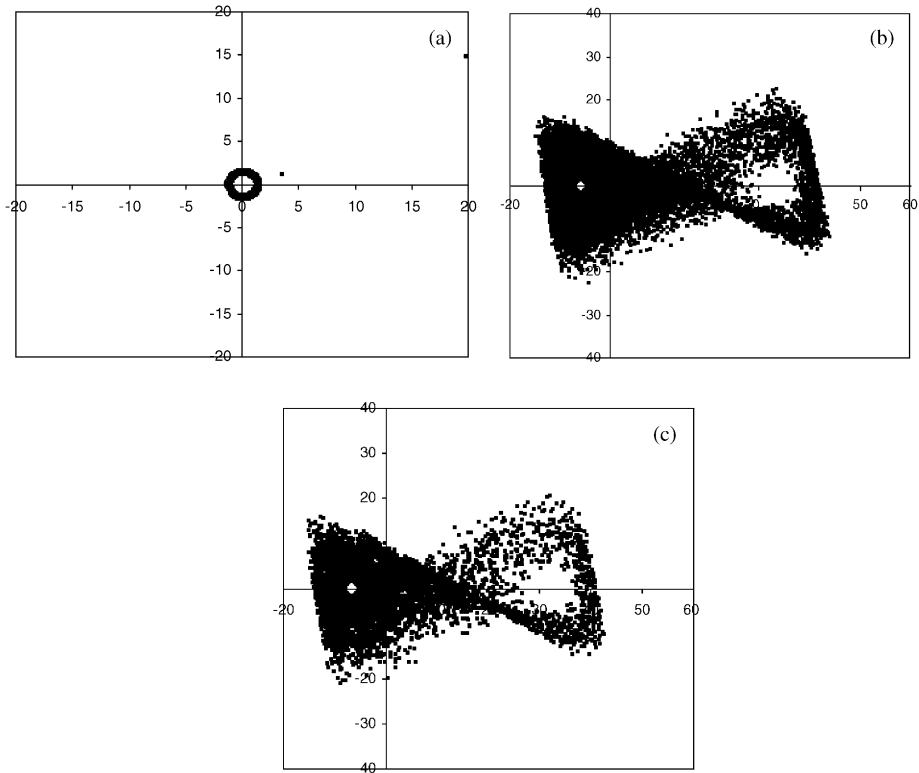
Fig. 4. (a–c) The phase–space plot for the $x(t)$ coordinate of system (12) for the same intervals as in Fig. 3. The plot is along the principal axis (see text).

This system can also be treated with the multipole technique.

As a first step, we construct the phase–space plot of the x-coordinate. Fig 4 shows the phase–space plot for the same three time segments treated in Ref. [14]. Not surprisingly, there is much resemblance between the trajectories (in this case in the x–z plane) and the phase–space plots for each of the three time segments. Moreover, as the last two time segments yield similar trajectories, they also yield similar phase–space plots. However, the similarity between the two trajectories cannot be described by two approximately, equal correlation dimensions, since the correlation dimension cannot be defined for the approach to a fixed point. On the other hand, the resemblance between the two phase–space plots is characterized by two approximately identical quadrupole moments (see Table 2).

The difference between the first two time segments is in the case of the trajectories represented by two rather different dimensions (1.35 and 1.78, respectively) and in the case of the phase–space plots reflected by two rather dissimilar quadrupole moments (1.2 and −83, respectively).

But the multipole moments add some additional information about the distribution of the data points which is not available from the correlation dimension.

Table 2
Summary of the fractal dimension d_f and various multipoles for system (13) for the three time segments. For comparison the results for the Rössler and Lorenz attractor are given

	Number of points	d_f	Q_{xx}	Q_{yy}	T_{xxx}	T_{yyy}	κ_x	κ_y	κ_x/κ_x
RL I	5995	1.36	0.38	1.2	0.35	−0.15	0.51	0.49	0.96
RL II	25500	1.78	261	−83	18309	−92	0.12	0.11	0.94
RL III	8500	n.a	297	−98	19487	−151	0.11	0.11	0.95
Rössler	40000	2.13	255	−127	1465	0.9	0.05	0.50	9.80
Lorenz	40000	2.07	508	−186	−32	13	0.04	0.08	2.02

In Fig. 5, we display for each of the three time segments the point density around the two principle axis of the phase–space plot. The symmetry along the y-axis and the lack of symmetry in the two latest time segments along the x-axis is evident. Some similar symmetry/asymmetry also appears in the trajectories.

The lack of symmetry (large skewness) along the x-axis for the last two time segments is reflected by the large octupole moments $T_{xxx}(\sim 10^4)$, whereas the near symmetry (small skewness) along the y-axis is reflected by the much smaller values for the octupole moments T_{yyy} for the three time segments ($\sim 10^2$).

It is noteworthy that the second and third time segments have approximately the same kurtosis along the x-axis (κ_x) and along the y-axis (κ_y), but a much higher x- and y-kurtosis for the first time segment. This reflects the small spread of data points around the origin of the principal axis during the first time segment, and their subsequent dispersion during the second and third time segments. It is remarkable that the ratio of the y- to x- kurtosis (κ_y/κ_x) stays almost constant and close to one at all times. This value is much closer to the value of (κ_y/κ_x) for the Lorenz attractor than for the Rössler attractor (2.02 and 9.80, respectively) and reflects the overall resemblance of the combined system considered with the Lorenz attractor rather than with the Rössler attractor. This resemblance with the Lorenz attractor is expected due to the small α value, but is not revealed by either the rather identical correlation dimensions for these two attractors or their quadrupoles.

4. Application to the Diamond study

We shall in the following demonstrate how the multipoles perform as predictors for mortality in the group of survivors after acute myocardial infraction in the Diamond study [12].

In this study 446 survivors of acute myocardial infarction (AMI) were enrolled. Different methods of analyzing HRV were compared with respect to predictive power of death after AMI. HRV was obtained from consecutive R–R intervals from 24 h ECG recordings 5–10 days after AMI. The mortality was 25.6% after a follow-up of 685 ± 360 days (114 died).
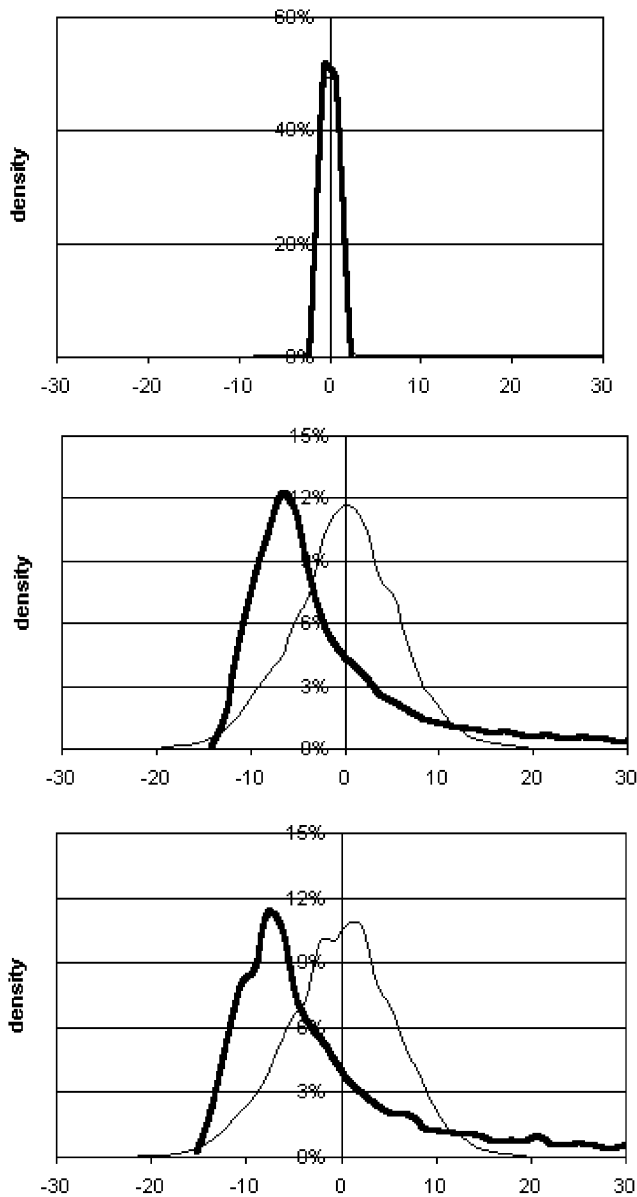
Fig. 5. The point density distribution along the two principal axis of the phase–space plot in Fig. 4. The time intervals are as in Fig. 3 (thick curve: along the x-axis; thin curve: along the y-axis).

By calculating the quadrupole moments for all 446 recordings one can achieve a first separation into a high-risk group ($Q_{yy} > -1400$[1]) and into a low-risk group

---

[1] The quadrupoles are given in ms^2.

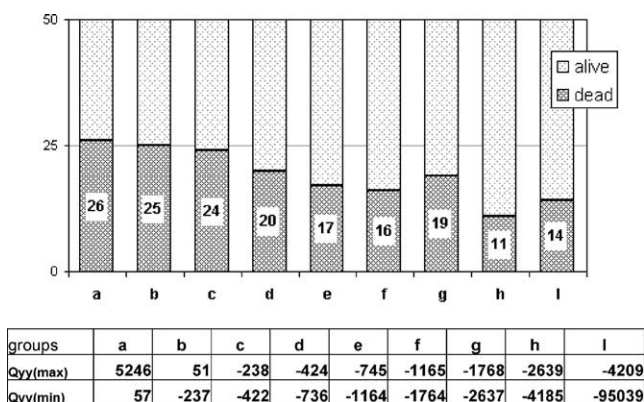| groups	a	b	c	d	e	f	g	h	I
Qyy(max)	5246	51	-238	-424	-745	-1165	-1768	-2639	-4209
Qyy(min)	57	-237	-422	-736	-1164	-1764	-2637	-4185	-95039

Fig. 6. Q_{yy} as a risk factor. The patients are grouped into groups of 50 according to decreasing Q_{yy}.

($Q_{yy} < -1400$). This first separation has a better overall predictive accuracy than the standard deviation of the RR intervals (SDNN), which is the conventional HRV marker. In Fig. 6, we show that the mortality is decreasing with increasing values of Q_{yy}.

In order to appreciate the significance of the octupole moment we show in Fig. 7 the phase–space plot from two of the recordings from the Diamond study. They have approximately the same value for the quadrupole moment but very different octupole moments. Fig. 7a shows the phase–space plot of a survivor with the highest concentration of data points on the positive part of the x-axis, with the interpretation that the heart beats for extended periods with a low pulse rate (large RR intervals), where as Fig. 7b shows the plot of a deceased individual with the larger part of data points concentrated on the negative part of the x-axis, i.e., the heart is beating with a high pulse rate for extended periods. In Fig. 8a, we show the separating power of the octupole T_{xxx}.[2] A similar analysis can be applied to the octupole moment T_{yyy} on the y-axis. The main result is that a high concentration of phase–space points on the positive y-axis (positive y-skewness) indicates a slow decrease and a fast increase in the heart rate which is a sign of impaired sympathetic and\or parasympathetic nervous system. Negative skewness on the y-axis, implying a slowly increasing and fast decreasing pulse, is hence one of the indications for a well-functioning heart function, which is also confirmed by the histogram in Fig. 8b.

The additional octupole moments add very little to the overall predictive accuracy in the Diamond study and therefore are excluded here.

Instead of seeking out the significant ones among the 16 hexadecupole moments, we shall use the kurtosis as mentioned above which is a powerful risk marker in the Diamond study. Table 3 lists 10 individuals with low-risk quadrupole and octupole moments but with a high value for concentration both around the x-axis as well as the y-axis and with a mortality of 90%, remarkable high relative to the overall mortality of 30%.
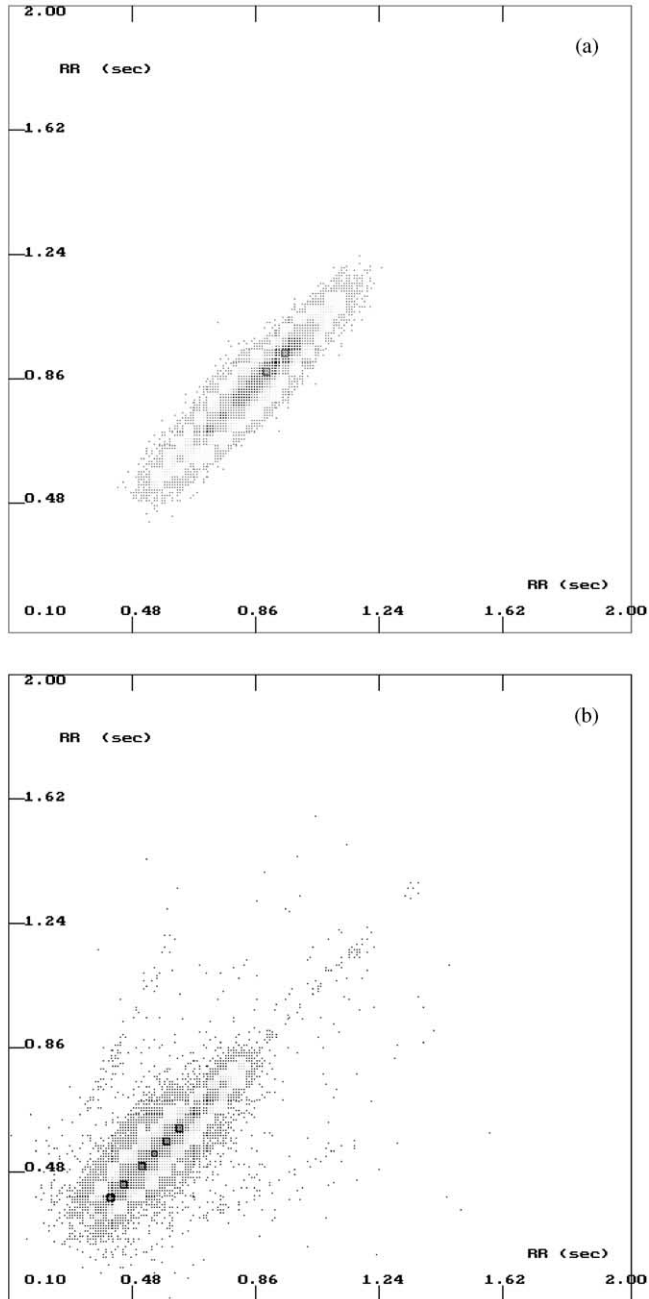
---

[2] The octupoles are given in $ms^3/10^3$.

Fig. 7. Phase–space plots for survivor (a) and non-survivor (b). Both have approximately the same Q_{yy}.
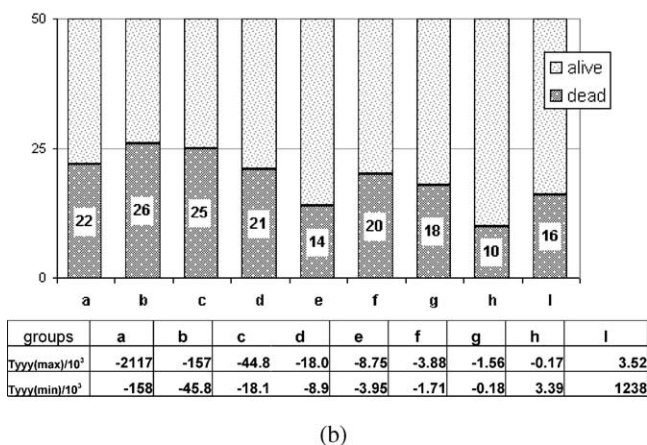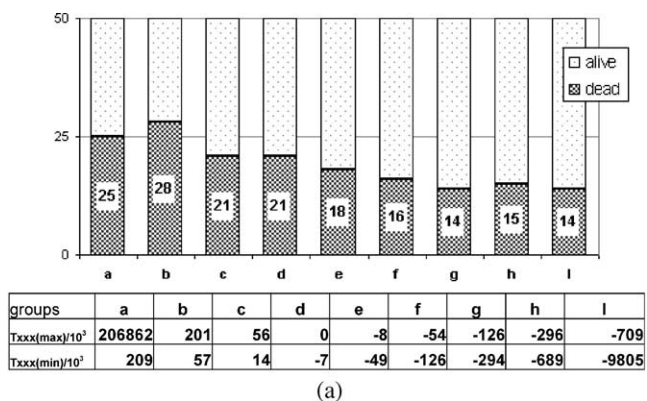
(a)

(b)

Fig. 8. (a) T_{xxx} as a risk factor. The patients are grouped into groups of 50 according to decreasing T_{xxx}. (b) T_{yyy} as a risk factor. The patients are grouped into groups of 50 according to increasing T_{yyy}.

Table 3
11 patients with low-risk quadrupole and octupole moments, but with high-risk kurtosis ratios

Patient #	Patient status	Q_{yy}	T_{xxx}	κ_y/κ_x
1	Deceased	−1828	−797	1.97
2	Deceased	−1560	−108	2.01
3	Deceased	−1797	−95	2.25
4	Deceased	−1856	−389	2.27
5	Deceased	−2101	−444	2.31
6	Deceased	−2637	−1160	2.36
7	Alive	−1635	−204	2.37
8	Deceased	−1525	−331	2.38
9	Deceased	−1926	−261	2.40
10	Deceased	−1702	−316	2.43
11	Deceased	−1426	−69	2.48

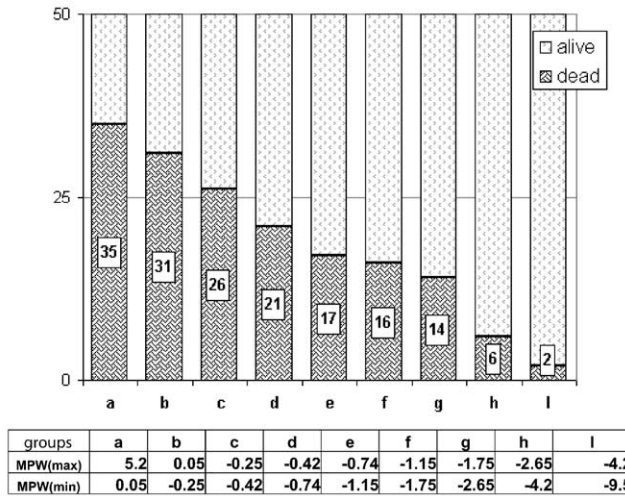| groups	a	b	c	d	e	f	g	h	I
MPW(max)	5.2	0.05	-0.25	-0.42	-0.74	-1.15	-1.75	-2.65	-4.2
MPW(min)	0.05	-0.25	-0.42	-0.74	-1.15	-1.75	-2.65	-4.2	-9.5

Fig. 9. MPW as a risk factor. The patients are grouped into groups of 50 according to decreasing MPW.

Combining by optimization (as for example in Ref. [15]) the various moments into one parameter we obtain a combined parameter with an improved predictive accuracy.

Fig. 9 shows the predictive potential of the optimized parameter, MPW (multipole moments weighted), where Q_{yy}, T_{xxx} and κ_y/κ_x are taken into consideration.

5. Discussion

We have studied two examples of non-stationary systems with rather complex time evolution.

The series of RR intervals is an excellent example of a non-stationary and non-linear time series with a very complex behaviour. It seems reasonable to expect that the regulation of the heart rhythm which is a very complex mechanism due to its dependence on many subsystems in the body can be described optimally only by a method which has a diversity of different parameters describing partly different behaviours of those subsystems.

The MPW performs better than the SDNN and the DFA which were superior among the methods compared in the study [8]. We conclude that the Multipole Method extracts information both in the frequency domain as well as in the time domain, and therefore performs better in prognostics than the traditional HRV methods, which are imbedded in one of the two domains.

The multipoles moments differ crucially from the SDNN which does not include any time-ordering (shuffling the RR intervals will result in almost the same value for SDNN), while the multipoles due to the very construction of the phase–space plot bear intrinsic time dependence.

We also studied a combination of two well-known chaotic attractors, the Lorenz and the Rössler attractor. We showed that a fractal dimension analysis only partly reflects the richness that the combined system exhibits.

Generally, the dimensional analysis is only feasible for systems which do not undergo marked changes in their time dependence. For those systems multipole analysis may reveal more details since it contains different moments describing different characteristics of the system studied.

References

[1] S. Thurner, M.C. Feuerstein, M.C. Teich, Phys. Rev. Lett. 80 (1998) 1544.
[2] Y. Ashkenazy, M. Lewkowicz, J. Levitan, H. Moelgaard, P.E. Bloch-Thomsen, K. Saermark, Fractals 6 (1998) 197.
[3] C.K. Peng, S. Havlin, H.E. Stanley, A.L. Goldberger, Chaos 5 (1995) 82.
[4] L.A. Nunes Amaral, A.L. Goldberger, P.C. Ivanov, H.E. Stanley, Phys. Rev. Lett. 81 (1998) 2388.
[5] S. Thurner, M.C. Feuerstein, S.B. Lowen, M.C. Teich, Phys. Rev. Lett. 81 (1998) 5688.
[6] K. Saermark, M. Moeller, U. Hintze, H. Moelgaard, P.E. BlochThomsen, H.V. Huikuri, J. Levitan, M. Lewkowicz, Fractals 8 (2000) 4.
[7] Y. Ashkenazy, M. Lewkowicz, J. Levitan, S. Havlin, K. Saermark, H. Moelgaard, P.E. BlochThomsen, M. Moeller, U. Hintze, H. Huikuri, Europhys. Lett. 53 (2001) 709.
[8] H.V. Huikuri, T. Seppanen, M.J. Kopistinen, K.E.J. Airaksinen, M.J. Ikaheimo, A. Castellanos, R.J. Meyerburg, Circulation 93 (1993) 1836.
[9] P.W. Kamen, A.M. Tomkin, Aust. NZ. J. Med. 25 (1995) 18.
[10] P.W. Kamen, H. Krum, A.M. Tomkin, Clin. Sci. 91 (1996) 201.
[11] M. Malik, Curr. Opinion Cardiol 13 (1998) 36.
[12] H.V. Huikuri, T.H. Mäkikallio, C.K. Peng, A.L. Goldberger, U. Hintze, M. Moller, Circulation 101 (2000) 47.
[13] M. Abramowitz, I. Stegun, Handbook of Mathematical Functions, Dover Publications, New York, 1970 (Chapter 26).
[14] K. Saermark, Y. Ashkenazy, L. Levitan, M. Lewkowicz, Physica A 236 (1997) 363.
[15] E. Kreyszig, Advanced Engineering Mathematics, Wiley, New York, 1998.